Terahertz Phase Contrast Imaging

Gretel M. Png[a,b], Samuel P. Mickan[a], Tamath Rainsford[a], Derek Abbott[a]

[a]Centre for Biomedical Engineering, School of Electrical and Electronic Engineering, The University of Adelaide, SA, 5005, Australia;

[b]Cooperative Research Centre for Sensor Signal and Information Processing, SPRI Building, Technology Park Adelaide, Mawson Lakes Boulevard, Mawson Lakes, SA 5095, Australia.

ABSTRACT

Terahertz imaging is presently in its exploratory stage. Although plots of time versus terahertz amplitude, and frequency versus terahertz magnitude are some of the most common ways of analyzing terahertz data, no standard rendering technique has been established. While existing methods are indispensable, improvements to how terahertz data is rendered and analyzed should be explored so that new techniques can complement existing ones and/or provide a means of displaying new information that existing methods cannot. This paper reports on one solution to terahertz imaging: an implementation of a new form of phase contrast imaging, which is based on a well-established technique for optical microscopy. This will provide us with a further way of interpreting information from terahertz imaging systems.

Keywords: Phase contrast, terahertz, T-rays, imaging

1. INTRODUCTION

Phase contrast is an optical method that enables the recovery of a specimen's phase information using an amplitude detector. It is a method that is traditionally employed in optical microscopy. Phase contrast was invented by Frits Zernike of the University of Groningen, the Netherlands; it is essentially a spatial analog of temporal heterodyne detection. Zernike first published his invention in 1934 where he described the use of phase contrast in microscopy.[1] This revolutionized the field of microscopy and earned him the Nobel Prize in Physics in 1953. Since its inception, the phase contrast method has become an integral part of optics, and phase contrast microscopes are not an unfamiliar sight in microscopy labs. In 2003, the phase contrast method entered the twenty-first century when the QPI (Quantitative Phase Imaging) algorithm was launched by IATIA Vision Sciences[2] in Australia. The QPI algorithm recovers the phase information of images obtained with a light microscope (non phase contrast microscope). This algorithm is the impetus for our study into an alternative phase retrieval method using terahertz (0.1 THz - 10 THz) data. The aim of this new method is to emulate optical phase contrast so that terahertz images can be enhanced. In addition, this method allows 3-Dimensional (3-D) rendering of the terahertz data, thus the implementation of more sophisticated 3-D graphics is a possibility. This paper will first give an overview of terahertz imaging with emphasis on the changes to a terahertz profile after propagating through a specimen. It will then present a novel method of manipulating terahertz data to emulate optical phase contrast. The paper concludes with a discussion of our results and suggestions for future work.

2. TERAHERTZ IMAGING

Terahertz (0.1 THz - 10 THz) Pulsed Imaging (TPI) is a technique used to obtain the broadband response of a specimen.[3–5] Short bursts of terahertz radiation (T-rays) are radiated on the specimen whereby the T-rays interact with and then leave the specimen. A 2-Dimensional (2-D) detector, such as a charge-coupled device (CCD) detects the transmitted T-rays as a $(N \times P)$ matrix; this is illustrated in Figure 1(a).

Further author information: (Send correspondence to Gretel Png)
E-mail: gpng@eleceng.adelaide.edu.au, Telephone: +61 (0)8 8303 6296
E-mail: spmickan@eleceng.adelaide.edu.au, Telephone: +61 (0)8 8303 4115
E-mail: tamath@eleceng.adelaide.edu.au, Telephone: +61 (0)8 8303 6393
E-mail: dabbott@eleceng.adelaide.edu.au, Telephone: +61 (0)8 8303 5748

Smart Structures, Devices, and Systems II, edited by Said F. Al-Sarawi,
Proceedings of SPIE Vol. 5649 (SPIE, Bellingham, WA, 2005)
0277-786X/05/$15 · doi: 10.1117/12.582582

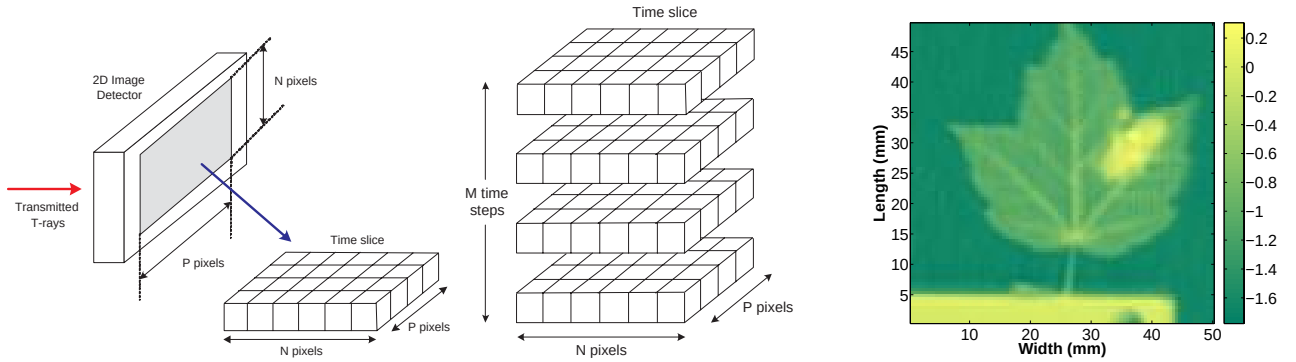

(a) 2-D terahertz data from CCD (b) 3-D terahertz data (c) One time slice of the terahertz matrix

Figure 1. (a) Transmitted T-rays are upconverted to the visible light band and captured by a charge-coupled device (CCD) as an image with $(N \times P)$ pixels for one instance of time. (b) By stacking the $(N \times P)$ images from the CCD, a 3-Dimensional data set is obtained via a pump-probe measurement technique. (c) One time slice of the terahertz data which was obtained via Terahertz Pulsed Imaging (in transmission mode). The time slice contains terahertz amplitude values. The image shows a considerable amount of the specimen's details. Such details act as the specimen's spatial fingerprints. A pseudo-color scheme is employed: bright areas signify high (positive) terahertz amplitude and dark areas signify low (negative) terahertz amplitude.

Stacking the sets of $(N \times P)$ matrices one on top of the other produces a $(M \times N \times P)$ matrix as shown in Figure 1(b). One horizontal time slice of the matrix is rendered in Figure 1(c). Although the image is not sharp, it is still possible to identify an insect, a leaf, a clamp holding the leaf and regions of free-space (air).

When T-rays interact with the specimen, the specimen's biological, structural and/or chemical properties *uniquely* alter the nature (e.g., amplitude attenuation, time delay) of the exiting T-rays. This unique alteration becomes a "fingerprint" of the specimen's properties. This fingerprint can be used in classification or identification applications. In Figure 1(c), the specimen's spatial fingerprint for one time slice is revealed. The fuzzy edges and artifacts in Figure 1(c) demonstrate that these terahertz images are limited by Signal-to-Noise-Ratio (SNR). Removal of background noise is required before spatial features can be extracted.[6]

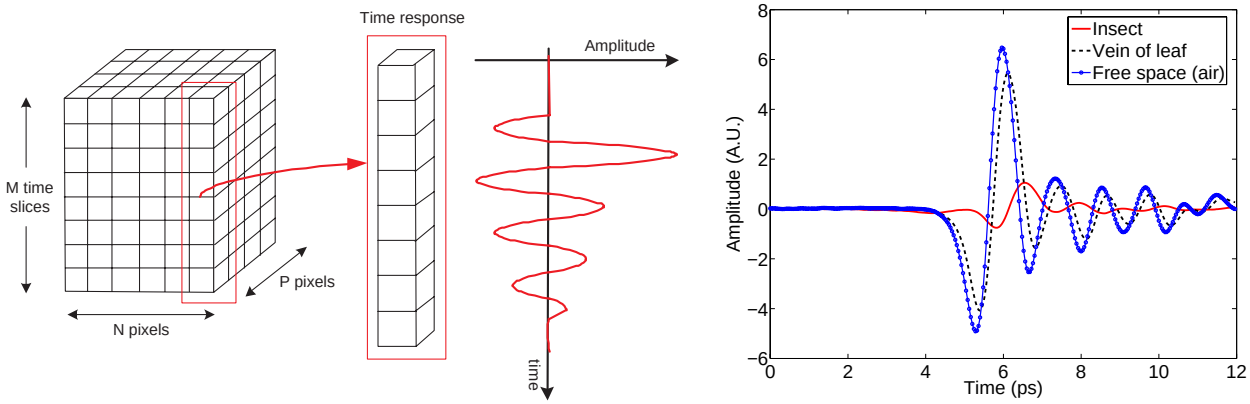

(a) Extracting a pixel's time response (b) The effect of the specimen on the terahertz profile

Figure 2. (a) A pixel's time response is stored as a $(M \times 1)$ column array. (b) The time response of 3 different pixels: insect, vein of leaf and free-space. The vein of the leaf (dashed plot) is fairly thin thus it delays the terahertz profile but does not significantly alter the amplitude. The insect (solid plot) could be thicker and/or have a higher refractive index than the leaf, thus the optical path length increases resulting in a significant delay of the time profile. The higher moisture content in the insect absorbs more T-rays, hence the greater amplitude attenuation of its time profile.

The temporal fingerprint is revealed by observing the time response of a pixel, i.e., a plot of the pixel's

($M \times 1$) time data as shown in Figure 2(a). Figure 2(b) shows the time response of three pixels from the leaf/insect specimen mentioned above. The pixels are of the insect, vein of the leaf and free-space. When compared to the free-space plot (solid-circle plot), the terahertz profiles after exiting the insect (solid plot) and leaf (dashed plot) are attenuated in amplitude; this is expected since T-rays are strongly absorbed by moisture. The terahertz profile for the insect is phase shifted more than the leaf's profile implying that the insect is thicker than the leaf and/or has a higher refractive index, which slows down the propagating T-rays. These time profiles can be Fourier transformed to obtain the broadband frequency response.

It is important to mention here that not all terahertz profiles are as easily interpreted. The polarity of the peak may change when the terahertz radiation propagates through different refractive indices. Pulse broadening may also occur due to dispersion of the T-rays by the specimen.[5] In Figure 2(b), the terahertz profile through the insect (solid plot) is deformed compared to the original free-space pixel. Negative group velocity may be present, which causes the first trough at 4 picoseconds.[7,8] Assumptions about the time profile will be emphasized when phase retrieval via terahertz imaging is explained in Section 4.

3. PHASE RETRIEVAL TECHNIQUES

Zernike's groundbreaking hardware-based optical phase contrast method is still reliable and applicable today, but its lack of quantitative phase information has spurred investigation into quantitative phase retrieval methods. The software-based Quantitative Phase Imaging (QPI) algorithm is of particular interest in this paper because it can recover quantitative phase information retroactively. For completeness, a short review of the QPI algorithm is provided in this paper. The most influential phase retrieval method in this investigation, however, is Zernike's optical phase contrast, hence a substantial portion of this paper is allocated to explaining how optical phase contrast has influenced this investigation.

3.1. Optical Phase Contrast

Zernike's optical phase contrast method is based on the effect of light passing through a phase object*. When light passes through free-space/air (surround path), the phase and amplitude information in the light wave is unaltered. When light passes through a phase object (particle path), the amplitude of the light wave is slightly attenuated due to energy loss. The light wave also slows down due to the refractive index of the phase object; the amount of delay introduced will also depend on the object's thickness. The difference in phase between the surround and particle paths is approximately a quarter of the wavelength. The human eye, however, can only sense amplitude and color differences when both the surround and particle paths are in phase. Since the surround and particle paths are out of phase by a quarter wavelength, the two paths appear identical to the eye[10] and contrast is lost. Phase objects therefore appear invisible under a conventional light microscope. Figure 3(a) illustrates the phase difference in the two paths. Note that the subtraction of the particle path from the surround path results in a wave that is a quarter of the wavelength out of phase to the surround path.

Zernike discovered that in order to enhance the contrast, the surround path can be manipulated to bring it back in phase with the particle path, resulting in the visibility of the phase object. The manipulation involves inserting a phase annulus and a phase plate into a conventional light microscope. The phase (or condenser) annulus creates a defocused, parallel light wavefront that illuminates the phase object.[11] The phase plate retards or advances the surround light by a quarter wavelength, and attenuates its amplitude. The choice of retardation or advancement is application specific. When the two paths recombine at the microscope's eyepiece, they are in phase (Figure 3(b)) and any amplitude changes in the particle path can be detected by the eye. Phase objects are therefore visible under phase contrast microscopy.

*An object that is not observable (transparent, invisible) because it does not provide contrast with the background. It does however cause phase modulations in the irradiated light wave, whereby these phase modulations are due to either the different refractive index of the object from air, the thickness of the object, or both.[9]

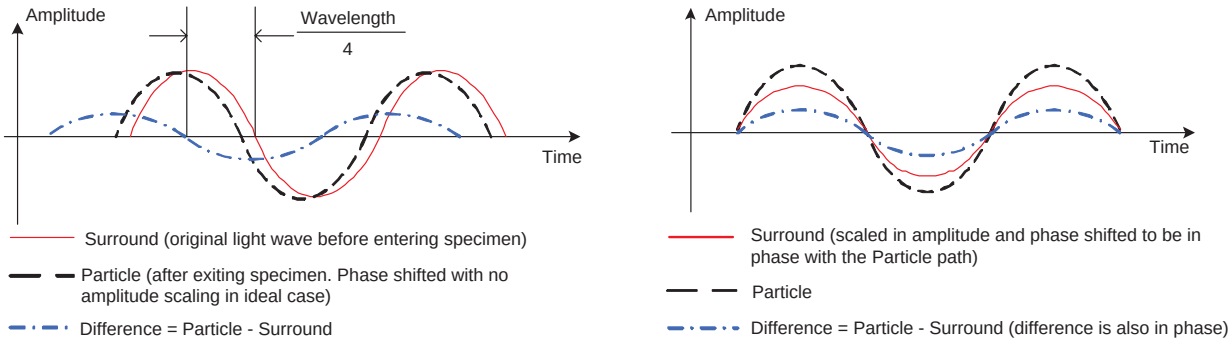

(a) Without phase adjustment (b) After quarter wavelength adjustment

Figure 3. (a) The particle path is phase shifted and not scaled in amplitude in the ideal case. The amplitude difference of the surround and particle paths is out of phase with the surround path, thus the particle path is not observable by the human eye. (b) With the quarter wavelength adjustment, both the surround and particle paths are now in phase; their phase difference is zero (constructive interference). When the surround and particle paths have the same amplitude, their amplitude difference is zero. When the surround and particle paths have different amplitudes, their amplitude difference is non-zero. The human eye is able to detect these amplitude changes (after Bennett[10]).

3.1.1. Applicability to Terahertz Imaging

The phase delay encountered in optical phase contrast is the same as the time delay encountered in T-rays. Recall that in Section 2, the terahertz profile is altered after propagating through a specimen. Comparing the dashed plots in Figures 2(b) and 3(a), we see the common phase offset phenomenon. Recall also that in Section 2, the altered terahertz profile is a "fingerprint" of the specimen. This means that features such as shape, amplitude, and time shift of the profile can act as individual fingerprints. The time difference between the peaks of the solid-circle and dashed plots in Figure 2(b) is therefore a fingerprint. The amplitude difference between the peaks of the solid-circle and dashed plots in Figure 2(b) is another fingerprint.

The goal of optical phase contrast is to align the surround and particle waveforms so that they are in phase and can recombine constructively in time. Could this alignment idea be applicable to terahertz data considering the 3-Dimensional terahertz data has both temporal and spatial information? In this paper, temporal alignment

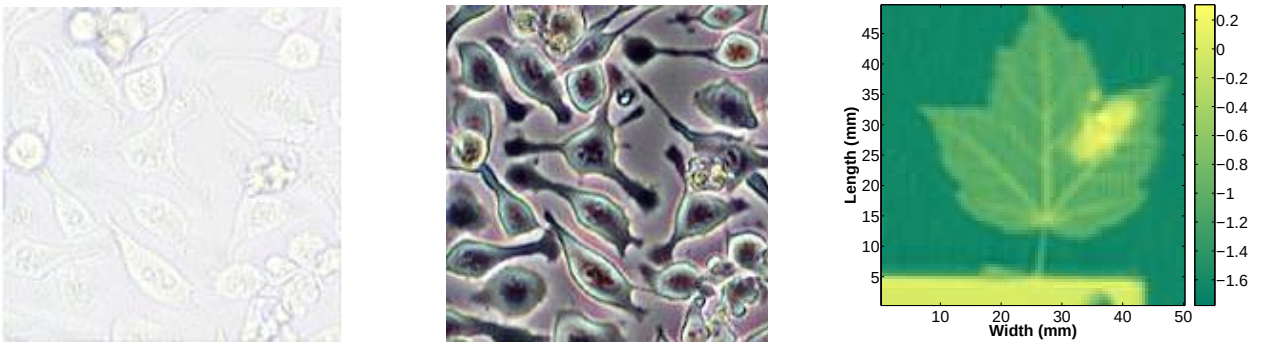

(a) From light microscopy (b) From phase contrast microscopy (c) From terahertz spectroscopy

Figure 4. (a) and (b) illustrate the image quality from a light microscope and a phase contrast microscope. The brightfield image from a light microscope looks washed-out and lacks contrast. The image of the same cells (without staining) from a phase contrast microscope has far more contrast and reveals edges that highlight structures within a cell and delineates one cell from another (after Nikon Microscopy[11]). (c) A terahertz image, Figure 1(c), is reproduced here. On its own, this image shows considerable detail of the insect and leaf. Compared to the optical phase contrast image, Figure 4(b), the lack of sharpness is pronounced.

of terahertz data has been investigated and found to be plausible. It is however not in the scope of this paper to discuss the combined effect of aligning temporal and spatial data as further investigation is required. The method used to implement temporal phase contrast with terahertz data is reported in Section 4.

As a final note about optical phase contrast, its image quality should be mentioned. Without any form of staining, optical phase contrast images show remarkable contrast with crisp edges and depth of field, delineating regions of differing thickness and/or refractive index. Figures 4(a) and 4(b) show the distinct improvement in contrast of cells, which are a common phase object. The details of the cells are heightened with optical phase contrast microscopy.

The quality of optical phase contrast images is a benchmark for image quality. The quality of post phase-retrieved images via terahertz imaging would be expected to be as good, if not better.

3.2. Quantitative Phase Imaging (QPI)

Quantitative Phase Imaging (QPI) is an algorithm that recovers quantitative phase information lost in brightfield microscopy images.[2] The algorithm is based on deterministic phase retrieval formulated by Teague.[12] Teague proposed that for a light wave propagating in the $+z$ direction, a paraxial approximation of the time-averaged Poynting vector $\langle S \rangle$ is

$$\begin{aligned} \nabla \cdot \langle S \rangle &= \nabla_{\perp}(\mathbf{I_0} \nabla_{\perp} \phi) \\ &= -(\frac{2\pi}{\lambda}) \frac{\partial \mathbf{I}}{\partial z} \end{aligned} \tag{1}$$

where $\mathbf{I_0}$ is the irradiance over a plane, i.e., a focused brightfield image, and $\frac{\partial \mathbf{I}}{\partial z}$ is the longitudinal derivative (rate of change in the $+z$ direction) of the same brightfield image. Therefore, $\frac{\partial \mathbf{I}}{\partial z}$ is the difference between the focused brightfield image and a slightly defocused version.[13] From Equation 1, Paganin and Nugent[14] formulated that the phase ϕ can be recovered by

$$\phi = -k \frac{1}{I_0} \nabla_{\perp}^{-2} (\frac{\partial \mathbf{I}}{\partial z}). \tag{2}$$

The solution for ϕ is unique and is the basis for the QPI algorithm.

(a) Original image (b) QPI processed image

Figure 5. (a) Original image of a fossilized leaf occluded by coal dust. Removal of the dust is not possible without destroying the leaf's information underneath it. (b) Occluded parts of the image are extracted and the phase recovered using the QPI algorithm (after Barone-Nugent *et al.*[13]).

Figure 5 demonstrates the power of the QPI algorithm. The algorithm not only recovers the phase, but also enhances the image by recovering the phase information of occluded regions. Furthermore, the image quality is as good as optical phase contrast.

4. PHASE RETRIEVAL USING TERAHERTZ IMAGING

In Section 2, the temporal fingerprint of the specimen was discussed. Features such as time delay (phase shift) and amplitude attenuation of the time profile are suitable for identifying the specimen. In general, the time delay of an electromagnetic ray is related to two factors: (i) the optical path length and speed of the ray, and (ii) the refractive index of the medium through which the ray propagates.[9] The amplitude attenuation of an electromagnetic ray is related to the attenuation coefficient of the medium. Put simply, the time delay experienced by the ray is affected by the thickness and refractive index of the medium, while the amplitude attenuation tells us how absorptive (opaque) the medium is. Applying this theory to terahertz data with the assumption that the terahertz profiles are not deformed or inverted, means:

1. A profile for free-space needs to be identified and used as a reference.
2. The optical path length across the specimen can be obtained by extracting the peaks of the time profiles and calculating their time delay with respect to the reference.
3. The specimen's opacity to T-rays can be obtained by calculating the amplitude difference of the profiles with respect to the reference.

The terahertz data used in this investigation has size $300 \times 100 \times 99$. This means there are 300 amplitude values per pixel (time domain), and each time slice contains 100×99 pixels (spatial domain). One time slice was shown earlier in Figure 1(c) where $N = 100, P = 99$. It is apparent from this figure that the reference (free-space) pixel should be somewhere in the upper left or upper right corner. The low SNR however makes it difficult to pin-point a particular pixel as the reference. To overcome this, peak detection was performed on every pixel in the time domain, i.e., the peak of each 300×1 array was found. The peak detection extracted from each pixel the time occurrence and value of the peak amplitude, thus generating two 100×99 matrices. From each matrix, 15 neighboring pixels that correspond to the top left corner of Figure 1(c) were selected and used to average the free-space amplitude I_{ref} and propagation time τ_{ref}.

In this investigation, it was assumed that the peaks of the leaf's time profiles did not suffer from changes in polarity, and that pulse broadening did not adversely affect the shape of the profile. These assumptions were adopted because the leaf has a higher refractive index than air, so the T-rays have propagated through three media (air-leaf-air) and the polarity of their time profiles were unaltered upon exiting the leaf. The leaf used in this analysis was dry, thus it had minimal water content; strong water absorption that causes deformation of the profile was not expected. Dispersion caused by internal reflection was ignored due to the thinness of the leaf. The insect, being thicker and/or denser than the leaf, has caused some pulse broadening in the terahertz profile as seen by the solid plot in Figure 2(b). The polarity of the peak was expected to be inverted (a trough) because the T-rays have propagated through four media (air-insect-leaf-air). Referring to Figure 2(b), the trough at around 6 picoseconds seems to be the one of interest. This trough, however, occurs before the peak of the free-space profile (solid-circle plot) which gives a false impression of negative group velocity. The trough was therefore ignored in this initial analysis. The positive peak (after the peak of the free-space profile) was chosen instead, and the insect and the portion of leaf beneath it were treated as one object.

While performing peak detection, it was observed that artifacts in the terahertz data affected the extraction of peak values. For example, Figure 6 shows a section of the time profiles of free-space and leaf pixels. Leaving aside the artifact plot (leftmost plot), the peaks of the free-space and leaf pixels differ noticeably albeit by a small amount (around 0.1 Arbitrary Units at least). Notice the artifact plot can be easily mistaken as a leaf plot because of its lower amplitude. This artifact also occurs before the peak of the free-space data. Multiple artifacts were present in the terahertz data, which confused the peak detection algorithm. To remove the artifacts in this investigation, peaks that occurred before τ_{ref} were ignored in this investigation.

Using the 100×99 matrix containing the time information of the peaks, the propagation time of each pixel with respect to τ_{ref} is given by

$$\text{Relative propagation time, } \tau_i = |(\text{time occurrence of peak } i) \ - \tau_{\text{ref}}|\,, \text{ for } i \,\epsilon\, 1, \cdots, N \times P. \tag{3}$$

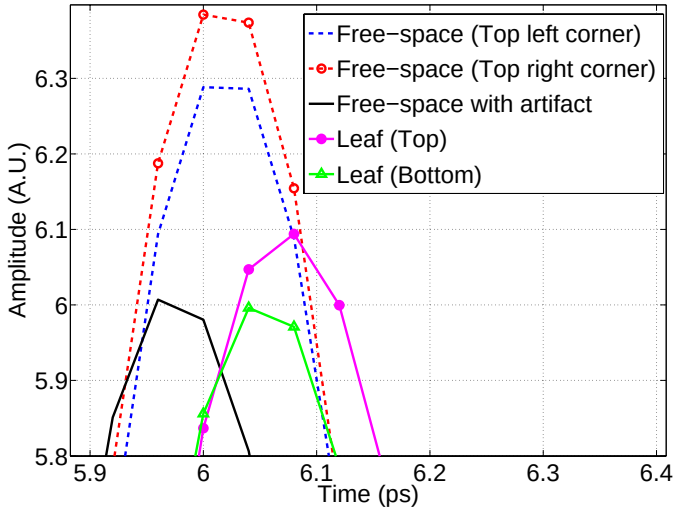

Figure 6. Peak amplitudes of the time profiles from 5 different pixels is shown. The dashed plots are the peaks of two arbitrary free-space pixels without artifacts. The leftmost solid plot is from a free-space pixel containing an artifact. The remaining two plots are of leaf pixels. The free-space plots (without artifact) have the highest amplitude and are easy to distinguish from the other plots. The artifact plot (leftmost plot) has a much lower amplitude and masks this plot as a leaf plot. The peak of the artifact plot also occurs before the peaks of the free-space plots, giving the false impression of negative group velocity.

The optical path length at each pixel is given by

$$\text{Optical path length, } d_i = \text{speed of light, } c \times \text{relative propagation time, } \tau_i, \text{ for } i \,\epsilon\, 1, \cdots, N \times P \tag{4}$$

where τ_i in this investigation is relative to τ_{ref}.

Using the 100×99 matrix containing the amplitude information of the peaks, the amplitude difference with respect to I_{ref} is given by

$$\text{Relative amplitude, } I_i \quad = \quad |I_{\text{ref}} - (\text{peak amplitude at pixel } i)|\,, \text{ for } i \,\epsilon\, 1, \cdots, N \times P. \tag{5}$$

The relative amplitude I_i tells us how absorptive the medium is to T-rays. If I_i is large, then large amounts of T-rays have been absorbed by the medium, hence low amounts of T-rays captured by the terahertz detector. If I_i is small, then the T-rays propagate through the medium without being absorbed. I_i can therefore be used to set the opacity of a pixel such that I_{ref} implies zero opacity (free-space is transparent) and $\max[I_{i\,\epsilon\,1,\ldots,N\times P}]$ implies unity opacity (opaque). As seen in Figure 6, the peak amplitudes of the free-space pixels vary slightly (dashed plots). In order to correctly identify all free-space pixels based on their amplitudes, these pixels were treated as spatial noise pixels and standard spatial noise removal techniques such as sharpening filters, 8-adjacency and thresholding were applied.[15] Figure 7(a) shows the combined effect of opacity and normalized optical path length. The leaf's smaller veins (the upper half of the leaf) can be seen due to their opacity values. Their optical path lengths however are not distinct enough and are lost among the rest of the leaf's optical path lengths. This combined opacity and optical path length information enables rendering of the data as a 3-Dimension image in applications such as MATLAB, enabling the viewer two additional dimensions when examining the terahertz data.

4.1. Discussion of Results

Figure 7(a) is rendered in Figures 7(b)-7(d) from different azimuths and elevations. The main vein of the leaf appears as a raised "spine" in Figure 7(b). The height of this spine is exaggerated when compared to the rest of the leaf because of the small (millimeter) normalized optical path length. The optical path length of the insect, although much larger than the leaf, is more plausible since the insect is thicker than and/or has a higher

refractive index than the leaf. The raised triangular region on the left of Figure 7(d) is the leaf's stem. Its optical path length is emphasized since it is thicker than the leaf's veins. The stem is also quite likely to contain more moisture than the leaf and thus appears more opaque (less transmitted T-rays due to absorption by moisture). The rest of the stem that protrudes from the leaf was rendered as being transparent because these pixels were mistaken as free-space pixels when image enhancement was used to set the pixels' opacity. A depression in the middle of the insect can be seen in Figures 7(a) and 7(d). When compared to the amplitude image in Figure 1(c), it appears there may be some feature on the insect's body that was less thick. Since the actual leaf and insect specimens used in generating the terahertz data are no longer available and no optical record exists, verification of the accuracy of these results is not possible. Nonetheless, this investigation has produced a novel way of analyzing terahertz data and has generated optical path length and opacity information that is in accordance with the concept of phase contrast.

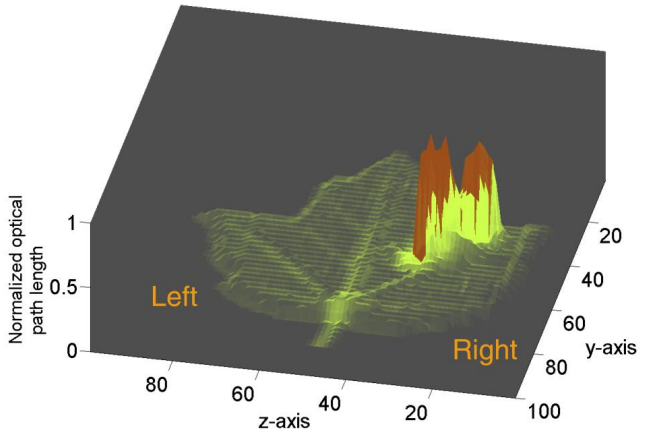

(a) Normalized optical path length and opacity

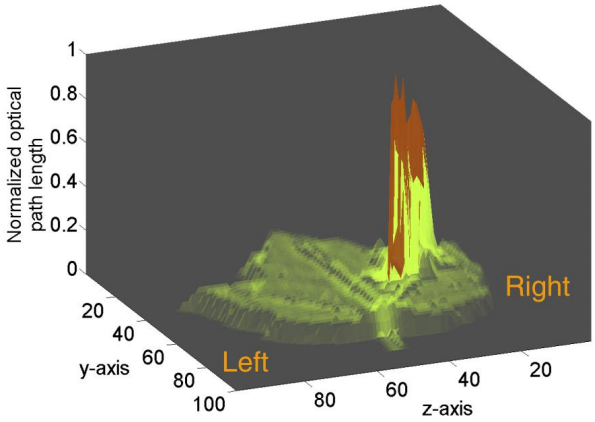

(b) View from left

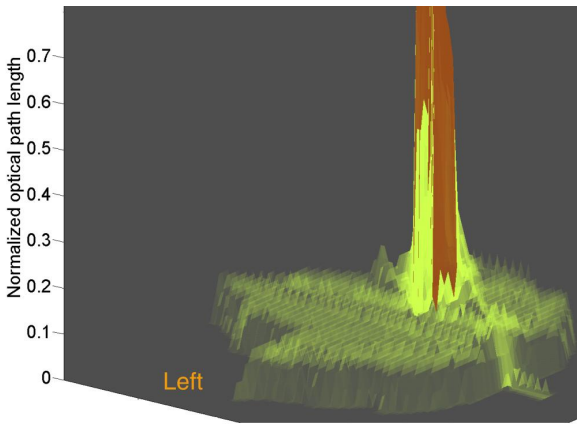

(c) View from left, zoomed

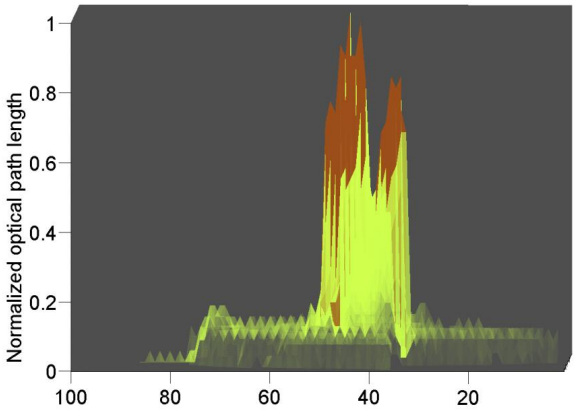

(d) View from right, zoomed

Figure 7. Different views of the final phase contrast image, containing both optical path length and opacity information. The optical path length is normalized and due to its fine resolution (in millimeters), the optical path length of the specimen is exaggerated. Figure (a) provided the best view of the leaf structure. Smaller veins are visible because of their low opacity values. The main vein in the middle of the leaf is wider and thicker, resulting in the spine-like ridge. At the base of the leaf is the stem which is thicker and more opaque, resulting in both a high optical path length and opacity to T-rays. The insect has a very high optical path length thus one would expect it was thicker and/or denser than the leaf. Its opacity with respect to T-rays is high implying it contained a fair amount of moisture which absorbed the T-rays.

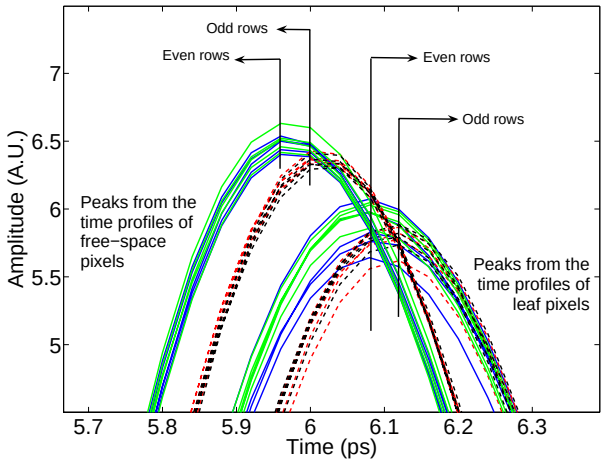

(a) Time offset comparison

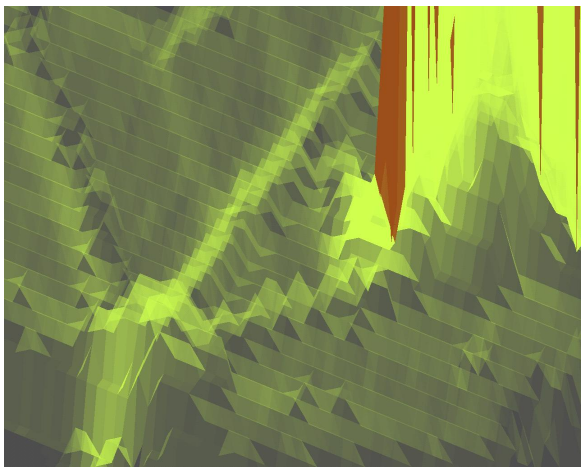

(b) Periodic ridges in amplitude image

Figure 8. (a) The dashed plots are the peak amplitudes of odd-rowed pixels while the solid plots are of even-rowed pixels. Regardless of the type of pixel (free-space or specimen), two adjacent pixels of the same type have a 0.4 picosecond offset in their peak amplitudes. (b) The time offset pattern appears as periodic horizontal ridges in the amplitude image.

During the investigation, one very peculiar artifact in the spatial domain was observed in the terahertz data. Taking several free-space pixels in Figure 1(c) as an example (say upper left corner), one would expect their terahertz amplitude peaks to occur around τ_{ref}. A plot of their free-space time profiles in Figure 8(a) shows this is indeed true. There is however a pattern: the peaks of all the even-rowed pixels occurred at $\tau_{\text{ref}} = 5.96$ picoseconds while all odd-rowed pixels occurred at 6 picoseconds. There is a 0.4 picosecond offset between the even and odd-rowed pixels, whereby 0.4 picosecond is the time resolution of the terahertz profile shown previously in Figure 2(b). This pattern was found to be common throughout the spatial domain regardless of the pixel type (free-space or specimen). This results in the spatial image having a periodic artifact that manifests itself as periodic horizontal ridges across the face of the image. This is observed in Figure 8(b), which is a zoomed version of Figure 7(a).

5. CONCLUSION AND FUTURE WORK

This investigation has shown it is feasible to apply the concept of optical phase contrast to terahertz imaging. By extracting the time peaks and amplitude differences from the specimen, it is possible to calculate the optical path length and opacity *to terahertz radiation*. A novel way of combining and rendering these two parameters enables the user to observe a specimen's broadband response 3-Dimensionally. It may also be possible to find the refractive index n, via optical path length $= n \times$ thickness of specimen. The combined effect of spatial and temporal phase shift will be the focus of future study.

ACKNOWLEDGMENTS

We wish to thank Bradley Ferguson for his advice. We also wish to thank The University of Adelaide, the Cooperative Research Centre for Sensor Signal and Information Processing, and the Sir Ross and Sir Keith Smith Fund for financial support. Rensselaer Polytechnic Institute, New York, is acknowledged for the leaf data.

REFERENCES

1. F. Zernike, "Beugungstheorie des Schneidenverfahrens und seiner verbesserten Form, der Phasenkontrast-methode," *Physica* **1**, pp. 689–704, 1934.
2. IATIA, "IATIA vision sciences." `http://www.iatia.com.au` (Accessed: November 3, 2004).

3. P. H. Siegel, "Terahertz technology," *IEEE Transactions on Microwave Theory and Techniques* **50**, pp. 910–928, March 2002.
4. S. Mickan, D. Abbott, J. Munch, X. C. Zhang, and T. van Doorn, "Analysis of system trade-offs for terahertz imaging," *Microelectronics J.* **31**, pp. 503–514, 2000.
5. D. M. Mittleman, R. H. Jacobsen, and M. C. Nuss, "T-ray imaging," *IEEE J. of Selected Topics in Quantum Electronics* **2**, pp. 679–692, September 1996.
6. B. Ferguson and D. Abbott, "Wavelet de-noising of optical terahertz pulse imaging data," *Fluctuation and Noise Letters* **1**(2), pp. L65–L69, 2001.
7. M. T. Reiten, D. Grischkowsky, and R. A. Cheville, "Terahertz pulse propagation in optical tunneling: causal vs. superluminal," in *Conference on Lasers and Electro-Optics (CLEO)*, p. 514, Optical Society of America, (Baltimore, MD, USA), 2001.
8. H. Cao, A. Dogariu, and L. J. Wang, "Negative group delay and pulse compression in superluminal pulse propagation," *IEEE J. of Selected Topics in Quantum Electronics* **9**, pp. 52–58, January/February 2003.
9. E. Hecht and A. Zajac, *Optics*, Addison-Wesley, Reading, Mass., 1987.
10. A. H. Bennett, H. Jupnik, H. Osterberg, and O. W. Richards, *Phase Microscopy: Principles and Applications*, John Wiley and Sons, New York, 1951.
11. Nikon, "Phase contrast microscopy." `http://www.microscopyu.com/articles/phasecontrast/phasemicroscopy.html` (Accessed: November 3, 2004).
12. M. R. Teague, "Deterministic phase retrieval: a Green's function solution," *J. Optical Society of America* **73**(11), pp. 1434–1441, 1983.
13. E. D. Barone-Nugent, A. Barty, and K. A. Nugent, "Quantitative phase-amplitude microscopy I: optical microscopy," *J. of Microscopy* **206**, pp. 194–203, June 2002.
14. D. Paganin and K. A. Nugent, "Noninterferometric phase imaging with partially coherent light," *Physical Review Letters* **80**, pp. 2586–2589, March 1998.
15. R. C. Gonzalez and R. E. Woods, *Digital Image Processing*, Prentice Hall, New Jersey, second ed., 2002.